Journal of Rock Mechanics and Geotechnical Engineering 15 (2023) 630–640

Contents lists available at ScienceDirect

Journal of Rock Mechanics and Geotechnical Engineering

journal homepage: www.jrmge.cn

Full Length Article

A generalized nonlinear three-dimensional failure criterion based on fracture mechanics

Zhaofeng Wang [a,b,c], Pengzhi Pan [a,b], Jianping Zuo [c,d,*], Yaohui Gao [e]

[a] State Key Laboratory of Geomechanics and Geotechnical Engineering, Institute of Rock and Soil Mechanics, Chinese Academy of Sciences, Wuhan, 430071, China
[b] University of Chinese Academy of Sciences, Beijing, 100049, China
[c] School of Mechanics and Civil Engineering, China University of Mining and Technology, Beijing, 100083, China
[d] State Key Laboratory of Coal Resources and Safe Mining, China University of Mining and Technology, Beijing, 100083, China
[e] Power China Huadong Engineering Corporation Limited, Hangzhou, 310014, China

ARTICLE INFO

Article history:
Received 2 November 2021
Received in revised form
10 March 2022
Accepted 15 May 2022
Available online 9 June 2022

Keywords:
Intermediate principal stress effect
Rock strength
Fracture mechanics
True triaxial compression

ABSTRACT

Based on fracture mechanics theory and wing crack model, a three-dimensional strength criterion for hard rock was developed in detail in this paper. Although the basic expression is derived from initiation and propagation of a single crack, it can be extended to microcrack cluster so as to reflect the macroscopic failure characteristic. Besides, it can be derived as Hoek–Brown criterion when the intermediate principal stress σ_2 is equal to the minimum principal stress $\sigma 3$ (Zuo et al., 2015). In addition, the opening direction of the microcrack cluster decreases with the increase of the intermediate principal stress coefficient, which could be described by an empirical function and verified by 10 kinds of hard rocks. Rock strength is influenced by the coupled effect of stress level and the opening direction of the microcrack clusters related to the stress level. As the effects of these two factors on the strength are opposite, the intermediate principal stress effect is induced.

© 2023 Institute of Rock and Soil Mechanics, Chinese Academy of Sciences. Production and hosting by Elsevier B.V. This is an open access article under the CC BY-NC-ND license (http://creativecommons.org/licenses/by-nc-nd/4.0/).

1. Introduction

Rock fracturing process under multiaxial stresses, especially the effect of stress on the rock brittle fracture, has become an significant subject in rock mechanics (Mogi, 1967; Pan et al., 2012). The magnitude and orientation of the principal stresses play important roles in changing the failure mode of rocks. The stiffness of testing machine apparently affects the post-peak stress–strain curves of brittle hard rocks under axial-strain-controlled loading (Cai et al., 2021). Conventional triaxial compression tests are often used to study the influence of confining pressure on rock failure. However, in the compression tests, the rock specimens is subjected to the same radial stress state. With the development of testing technique, a large number of true triaxial compression tests have been conducted to reveal the actual rock failure performance under principal stresses (Mogi, 1981, 2006; Geng and Xu, 1985; Takahashi and Koide, 1989; Chang and Haimson, 2000; Chen and Feng, 2006; Feng et al., 2016). More importantly, the special effect of intermediate principal stress (σ_2) on the rock strength has been observed and examined in these laboratory studies.

The intermediate principal stress effect revealed that hard rock strength increases and then decreases with the increase of σ_2. Based on the laboratory results, many theories have been proposed to interpret this effect. Earlier studies attributed this effect to the following three factors: uncertain anisotropy of rock (Böker, 1915), low accuracy of failure stress measurement (Murrell, 1965; Mogi, 1967; Chang and Haimson, 2000), and uneven stress distribution at the end of rock specimen (Jaeger and Hoskins, 1966). After the effect has been verified in true triaxial compression tests, this effect was considered as the influence of σ_2 on the effective normal stress over the failure plane (Mogi, 1967; Chang and Haimson, 2000), the effective shear strain energy stored in rock (Takahashi and Koide, 1989), or a kind of failure mode (Mogi, 2006; Feng et al., 2019). With deeper explanation and more profound understanding of this effect, various failure criteria considering the influence of σ_2 were proposed (Mogi, 1967, 1971; Aubertin and Simon, 1996; Ewy, 1999; Zhang and Zhu, 2007; Chang and Haimson, 2012; Ma et al., 2017; Wang et al., 2018, 2019; Feng et al., 2019). These interpretations and strength criteria mainly focus on the macroscopic failure

* Corresponding author. School of Mechanics and Civil Engineering, China University of Mining and Technology, Beijing, 100083, China.
E-mail address: zjp@cumtb.edu.cn (J. Zuo).

Peer review under responsibility of Institute of Rock and Soil Mechanics, Chinese Academy of Sciences.

https://doi.org/10.1016/j.jrmge.2022.05.006
1674-7755 © 2023 Institute of Rock and Soil Mechanics, Chinese Academy of Sciences. Production and hosting by Elsevier B.V. This is an open access article under the CC BY-NC-ND license (http://creativecommons.org/licenses/by-nc-nd/4.0/).

characteristics of rocks observed and summarized from laboratory results. However, they appear to ignore the physical mechanism induced by micro-fracturing.

On the other hand, based on the micro-fracturing mechanism, rock failure can be also studied from the theoretical perspective by establishing a theoretical model and making several assumptions. Some well-known strength criteria, such as the Griffith criterion (Griffith, 1921), modified Griffith criterion (McClintock and Walsh, 1962), and Wiebols–Cook criterion (Wiebols and Cook, 1968), were proposed based on pure mathematical derivation. A nonlinear strength criterion (Zuo et al., 2008) was derived for rocks based on fracture mechanics and two-dimensional (2D) crack model, which has a similar expression with the Hoek–Brown criterion (Hoek and Brown, 1980). This work was further extended to a three-dimensional (3D) crack model subjected to pseudo triaxial stress, namely $\sigma_2 = \sigma_3$. Based on that, the theoretical Hoek–Brown criterion was derived, and the physical meaning of the parameter m was explained (Zuo et al., 2015). The study of Zuo et al. (2015) is of great value for providing the basis and derivation of the Hoek–Brown criterion for intact rock using a fundamental and mechanically rigorous fracture mechanics approach (Brown, 2015). Renctly, Hoek and Brown (2019) and Rafiei Renani and Cai (2022) comprehensively reviewed the Hoek–Brown criterion from the perspectives of geological strength index (GSI) and jointed rock mass, respectively. Hoek and Brown (2019) pointed out that Zuo et al. (2008, 2015) showed a very similar equation which could be derived by analyzing the failure propagation of a penny-shaped crack in the triaxial stress field. Zuo and Shen (2020) investigated the micro-meso physical transformation mechanism and a theoretical model for brittle-ductile transition behavior of rocks in detail. Zhou et al. (2014) extended the nonlinear strength criterion to 3D conditions using a similar method. Through these theoretical studies, the gap between the physical mechanism and the macroscopic failure of hard rock can be completely or partially filled.

In this study, a 3D rock failure model containing a single microcrack subjected to true triaxial stresses is derived in detail based on fracture mechanics theory and the wing crack model. Then the model is extended to microcrack cluster to predict hard rock strength at macroscale. Based on several failure characteristics and reasonable assumptions, relations between the most favorable direction of microcrack cluster and intermediate principal stress coefficient are derived and examined based on the results of previous laboratory true triaxial compression tests. Finally, the intermediate principal stress effect on the hard rock strength is discussed and the physical meaning of the effect is revealed according to the above derivations and assumptions.

2. Fundamental hypotheses according to single penny-shaped crack model

The development of microcracks was the main reason of inelastic response of brittle or quasi brittle material (Tapponnier and Brace, 1976). Its strength decreased due to the existence of initial flaws or cracks (Jaeger et al., 2007). In this paper, it is assumed that the failure of hard rocks is caused by penny-shaped microcracks, which are widespread in many brittle materials (Paterson and Wong, 2005). Similar to Zuo et al. (2008), this paper makes two fundamental assumptions: (1) abundant penny-shaped microcracks are randomly embedded in the isotropic elastic material, and inelastic response is induced by the crack development; and (2) cracks are sparsely distributed, ignoring the interaction of these cracks.

Based on the above assumptions, the fracture model shown in Fig. 1 is considered, with a penny-shaped crack of radius a embedded in the isotropic elastic material matrix, loaded in the far field. The global and local coordinate systems of the crack are set as $Ox_1x_2x_3$ and $Ox'_1x'_2x'_3$, respectively. In the local coordinate system, the x'_2 axis is parallel to the normal vector of the crack, while both the x'_1 and x'_3 axes are parallel to the surface of the penny-shaped crack. Moreover, the x'_3 axis is coplanar with the x_2 and x_3 axes in the global coordinate system. In addition, the angle between the x'_2 axis and plane Ox_2x_3 is θ, while φ is the angle between the x'_3 and x_2 axes. Therefore, the set (θ, φ) can be adopted to describe the inclination of the penny-shaped microcrack in 3D space. The relation between the basic vector of the two coordinate systems is shown below:

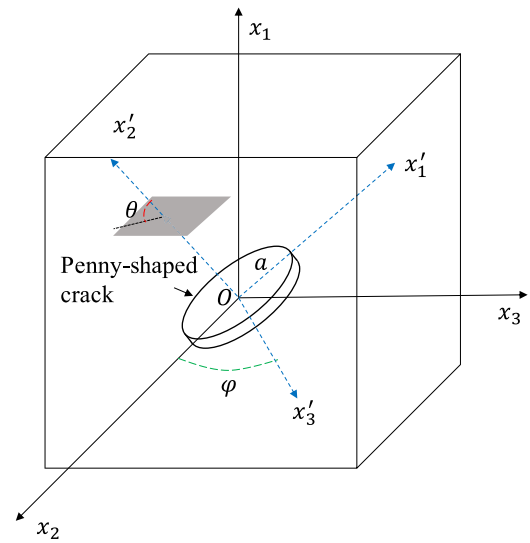

Fig. 1. Diagrammatic sketch of the fracture model, in which a penny-shaped crack is located in the material matrix. The global coordinate system ($Ox_1x_2x_3$) and the local coordinate system ($Ox'_1x'_2x'_3$) of the crack are also illustrated. The angle between the x'_2 axis and plane Ox_2x_3 is θ, and the angle between x'_3 and x_2 is φ.

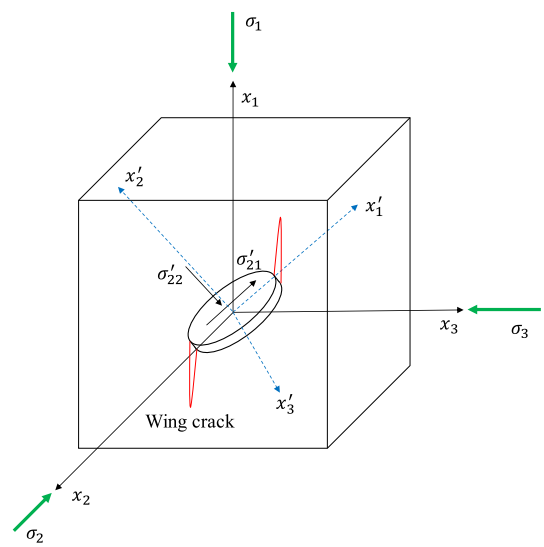

Fig. 2. Development of the penny-shaped microcrack. Secondary wing cracks form at the two tips of the microcrack due to the shear stress σ'_{21} on the surface of the penny-shaped microcrack. σ'_{22} is the normal stress on the surface. σ_1, σ_2 and σ_3 are loaded to the material matrix in the far field.

$$e'_i = \boldsymbol{g}_{ij} e_j \tag{1}$$

The relation between the stress components (positive in compression) of the two systems can be derived as follows:

$$\sigma'_{ij} = \boldsymbol{g}_{ik}\boldsymbol{g}_{jl}\sigma_{kl} \tag{2}$$

where

$$\boldsymbol{g}_{ij} = \begin{bmatrix} \cos\theta & -\sin\theta\sin\varphi & \sin\theta\cos\varphi \\ \sin\theta & \cos\theta\sin\varphi & -\cos\theta\cos\varphi \\ 0 & \cos\varphi & \sin\varphi \end{bmatrix} \tag{3}$$

Development of the penny-shaped microcrack is considered by the wing crack model (Horii and Nemat-Nasser, 1986; Wang and Shrive, 1993; Bobet, 2000), as shown in Fig. 2. When the penny-shaped crack propagates along x'_1, it is subjected to shear stress. However, it is subjected to tensile stress or traction when the crack propagates along the direction parallel to x_2. In addition, it is generally subjected to coupled tensile and shear stresses when the crack propagates between x'_1 and x_2. Therefore, the opening of the secondary wing cracks is caused by the shear stress or traction on the surface of the penny-shaped crack. The shear stress σ'_{21} and the normal stress σ'_{22} on the surface of the penny-shaped microcrack can be calculated as

$$\left.\begin{aligned} \sigma'_{21} &= \sigma_1\cos\theta\sin\theta - \sigma_2\cos\theta\sin\theta\sin^2\varphi - \sigma_3\cos\theta\sin\theta\cos^2\varphi \\ \sigma'_{22} &= \sigma_1\sin^2\theta + \sigma_2\cos^2\theta\sin^2\varphi + \sigma_3\cos^2\theta\cos^2\varphi \end{aligned}\right\} \tag{4}$$

According to the wing crack model (Horii and Nemat-Nasser, 1986; Wang and Shrive, 1993; Bobet, 2000), in-plane traction is always considered in the formation of the secondary wing cracks, while the out-plane traction should be ignored here. The stress intensity factor depends on the magnitude of the traction τ_t on the crack plane, which can be calculated below:

$$\tau_t = \tau - \tau_c = \tau - \mu\sigma_N = \sigma'_{21} - \mu\sigma'_{22} \tag{5}$$

where σ_N and τ are the normal and shear stresses on the shear plane, respectively; μ stands for the frictional coefficient; and τ_c is the shear strength on the plane, and it equals $\mu\sigma_N$ as the Mohr–Coulomb criterion is applied on the crack internal surface. Besides, the upper and lower sides of the pre-existing crack are disconnected. Therefore, the cohesion at the crack surface could be ignored. The stress intensity factor K_{II} for this in-plane shear crack can be calculated (Tada et al., 1973) as

$$K_{II} = \frac{4\tau_t}{2-\nu}\sqrt{\frac{a}{\pi}} \tag{6}$$

where ν is the Poisson's ratio, and a is the radius of the penny-shaped crack.

The propagation condition of the penny-shaped crack for the mixed fracture mode is defined (Kachanov, 1982) as follows:

$$K_{II} = \kappa K_{IC} \tag{7}$$

where K_{IC} is the fracture toughness for the mode I opening, which was determined by Zuo et al. (2008) as $2\sigma_t\sqrt{a/\pi}$, in which σ_t is the uniaxial tensile strength; and κ is the fracture coefficient depending on the mixed fracture criterion, for instance, $\kappa = 1$ for the maximum energy release rate criterion (Sih and Macdonald, 1974; Nuismer, 1975).

Combining Eqs. (4)–(7), the following equation can be obtained:

$$\begin{aligned} &(\beta+\mu s_1)\tan^2\theta + \left(s_2\sin^2\varphi + s_3\sin^2\varphi - s_1\right)\tan\theta \\ &\quad + \left(\beta + \mu s_2\sin^2\varphi + \mu s_3\cos^2\varphi\right) = 0 \end{aligned} \tag{8}$$

where $\beta = (1-\nu/2)\kappa$, $s_1 = \sigma_1/\sigma_t$, $s_2 = \sigma_2/\sigma_t$, and $s_3 = \sigma_3/\sigma_t$. Eq. (8) includes the possible crack inclination set (θ, φ) under different stress levels $(\sigma_1, \sigma_2, \sigma_3)$.

As θ is the angle between the local x'_2 axis and the plane Ox_2x_3, θ represents the inclination angle of the crack surface $Ox'_1x'_3$ relative to the x_1 axis or σ_1. The wing crack opening direction is coplanar with the x'_1 and x'_2 axes where the shear stress σ'_{21} and the normal stress σ'_{22} distribute, inducing the opening of the secondary wing crack. Moreover, the wing crack opening direction is also perpendicular to x_1 or σ_1. Therefore, φ can be considered as the rotation angle between the wing crack opening direction and x_3 or σ_3. For a given φ and far-field load set $(\sigma_1, \sigma_2, \sigma_3)$, as shown in Fig. 3, the range of $\tan\theta$, $\tan\theta_1$ and $\tan\theta_2$ can be calculated below:

$$\left.\begin{aligned} &\tan\theta_1 \le \tan\theta \le \tan\theta_2 \\ &\tan\theta_2 = \frac{s_1 - s_2\sin^2\varphi - s_3\sin^2\varphi + \sqrt{\left(s_1 - s_2\sin^2\varphi - s_3\sin^2\varphi\right)^2 - 4(\beta+\mu s_1)\left(\beta + \mu s_2\sin^2\varphi + \mu s_3\cos^2\varphi\right)}}{2(\beta+\mu s_1)} \\ &\tan\theta_1 = \frac{s_1 - s_2\sin^2\varphi - s_3\sin^2\varphi - \sqrt{\left(s_1 - s_2\sin^2\varphi - s_3\sin^2\varphi\right)^2 - 4(\beta+\mu s_1)\left(\beta + \mu s_2\sin^2\varphi + \mu s_3\cos^2\varphi\right)}}{2(\beta+\mu s_1)} \end{aligned}\right\} \tag{9}$$

In Fig. 3, $\alpha = \theta_2 - \theta_1$, which is used to represent the micro-failure orientation angle or azimuth under triaxial compression (Zuo et al., 2008). Based on Eq. (9), $\tan\alpha$ can be calculated as

$$\tan\alpha = \frac{\sqrt{\left(s_1 - s_2\sin^2\varphi - s_3\sin^2\varphi\right)^2 - 4(\beta+\mu s_1)\left(\beta + \mu s_2\sin^2\varphi + \mu s_3\cos^2\varphi\right)}}{\mu\left(s_1 + s_2\sin^2\varphi + s_3\cos^2\varphi\right) + 2\beta} \tag{10}$$

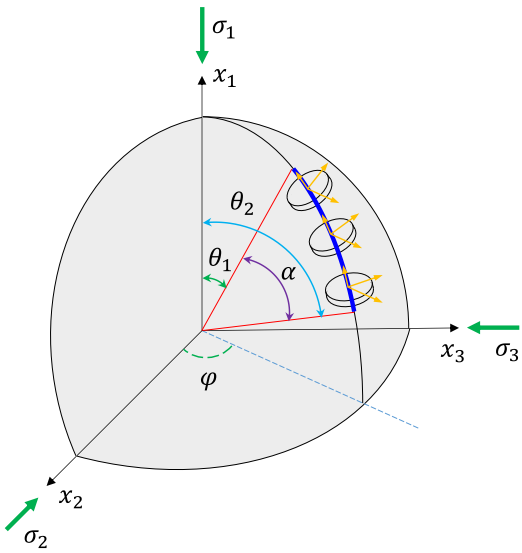

Fig. 3. The possible crack inclination angle θ in 1/8 of the unit sphere for a given φ and far-field load set (σ_1, σ_2, σ_3). The blue solid line represents the possible range, and penny-shaped cracks with their local coordinate systems are also illustrated. In addition, the upper and lower boundaries of the possible crack inclination angle, θ_2 and θ_1, are also shown.

The angle α represents the damaged portion of the internal microcrack, while the macroscopic damage occurs in the sector between θ_1 and θ_2 (Zuo et al., 2008), as shown in Fig. 3. Furthermore, $|\partial\alpha/\partial\sigma_1|$ can be used to measure the characteristic of damaged microcrack clusters that cause macr-failure considering both the magnitude and rate of change of this ratio. α can be replaced by $\sin\alpha$ as the angle between the final failure plane and σ_1 is relatively small (Zuo et al., 2015; Zuo and Shen, 2020). The following macro-failure measurement M can be obtained:

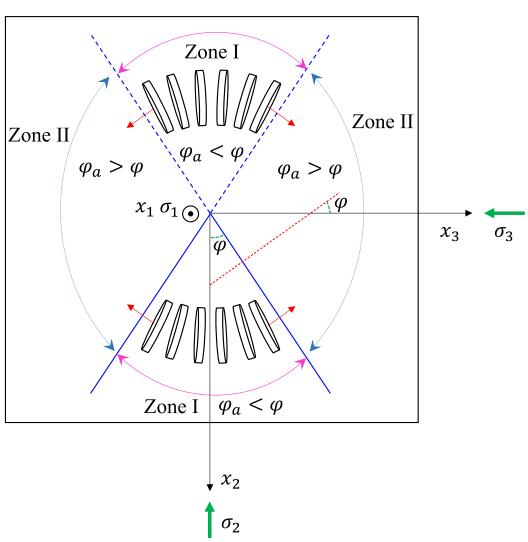

Fig. 4. Diagrammatic sketch of the opening tendency of a single crack. Zones I and II are the directional zones of opening and unopening tendency, respectively.

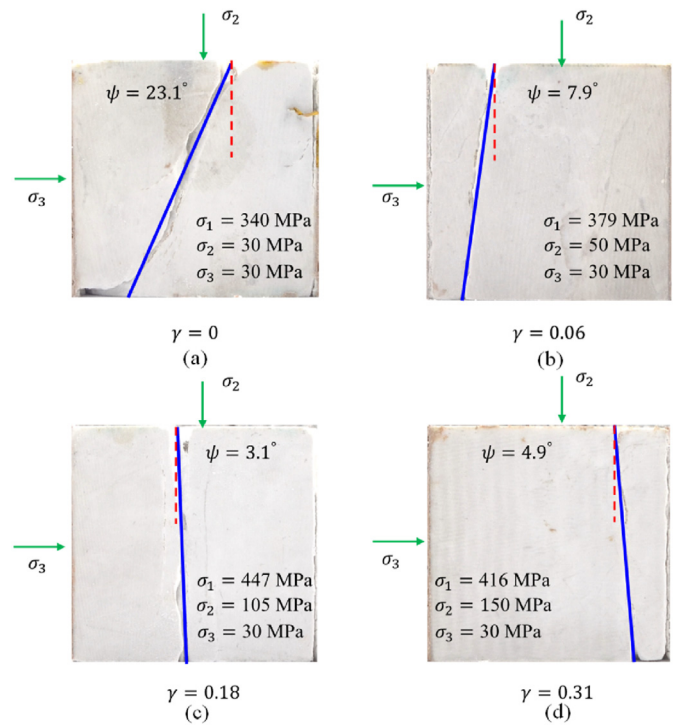

Fig. 5. Measurement of the macro-failure plane rotation angle ψ at different stress levels. It should be noted that ψ is calculated from a side image of the specimen and the spatial rotation is ignored: (a) $\gamma = 0$; (b) $\gamma = 0.06$; (c) $\gamma = 0.18$; and (d) $\gamma = 0.31$.

$$M = \left|\frac{\partial(\cos\alpha)}{\partial\sigma_1}\right| = \frac{\mu}{\sqrt{1+\mu^2}}\frac{\left(\cos\alpha\sqrt{1+\mu^2}\,/\mu - 1\right)^2}{2\left(s_2\sin^2\varphi + s_3\cos^2\varphi\right) + 2\beta/\mu} \tag{11}$$

In the uniaxial compression state, s_2 and s_3 equal 0, while s_1 is the ratio between the uniaxial compressive and tensile strengths, i.e. $s_1 = \sigma_c/\sigma_t$, which can be used to calculate the macro-failure measurement M_{uc} under uniaxial compression. The macro-failure measurement can quantitatively describe the macro-failure tendency for each rock type. When $M = M_{uc}$, the following relation can be obtained:

$$\sigma_1 = \sigma_2\sin^2\varphi + \sigma_3\cos^2\varphi + \sqrt{\frac{\mu}{\beta}\frac{\sigma_c}{\sigma_t}\sigma_c\left(\sigma_2\sin^2\varphi + \sigma_3\cos^2\varphi\right) + \sigma_c^2} \tag{12}$$

When $\sigma_2 = \sigma_3$ in the triaxial compression, Eq. (12) can be transformed into the following equation:

$$\sigma_1 = \sigma_3 + \sqrt{\frac{\mu}{\beta}\frac{\sigma_c}{\sigma_t}\sigma_c\sigma_3 + \sigma_c^2} \tag{13}$$

Eq. (13) is similar to the nonlinear strength criterion proposed by Zuo et al. (2008), which was strictly derived based on the theory of fracture mechanics and has a similar form with the Hoek–Brown criterion.

3. Extension to the strength of microcrack cluster

It should be noted that φ in Eq. (12) is obtained based on an assumption that there exists only one single crack embedded in the material matrix. In fact, the strength of rocks is determined by the behavior of microcrack cluster. As discussed above, in the condition

that σ_2 and σ_3 are constant, the larger the φ is, the larger the σ_1 will be based on Eq. (12). The opening tendency of a single crack is shown in Fig. 4 when φ stands for the material property. When the actual rotation angle φ_a is smaller than φ, the actual local strength σ_{1a}^s will be smaller than σ_1^s (calculated with φ from Eq. (12)). Therefore, the directional zone in which $\varphi_a < \varphi$ is considered to be of opening tendency. Oppositely, when $\varphi_a > \varphi$, the crack could be more stable due to the local strength σ_{1a}^s greater than σ_1^s, and thus the directional zone in which $\varphi_a > \varphi$ is considered to be of unopening tendency.

In the local area, the stress conditions are approximately the same when ignoring crack interactions. The microcrack cluster in this local area could influence the global bearing capacity. The opening of microcracks whose opening directions are in the directional zone of unopening tendency delays, and the other microcracks which open in the directional zone of opening tendency strengthen. Actually, the strength of microcrack cluster is determined by the maximum strength provided by the microcrack with the most favorable direction in the directional zone of opening tendency, which could be calculated below:

$$\sigma_1^s = \sigma_{1a}^s(\varphi_m) \tag{14}$$

where σ_{1a}^s can be calculated from Eq. (12), and φ_m is the most favorable direction. Apparently, φ_m is the upper limit of φ_a in the directional zone of opening tendency, and it is the assumed material property φ. Eq. (14) indicates that Eq. (12) is also suitable to describe the strength of microcrack cluster. The following strength criterion for microcrack cluster can be obtained by substituting Eq. (12) into Eq. (14):

$$\sigma_1 = \sigma_2 \sin^2\varphi_m + \sigma_3 \cos^2\varphi_m + \sqrt{\frac{\mu}{\beta}\frac{\sigma_c}{\sigma_t}\sigma_c(\sigma_2 \sin^2\varphi_m + \sigma_3 \cos^2\varphi_m) + \sigma_c^2} \tag{15}$$

Actually, the macro-failure is mainly influenced by the microcrack cluster instead of a single microcrack, indicating that φ_m can reflect the characteristics of macro-failure.

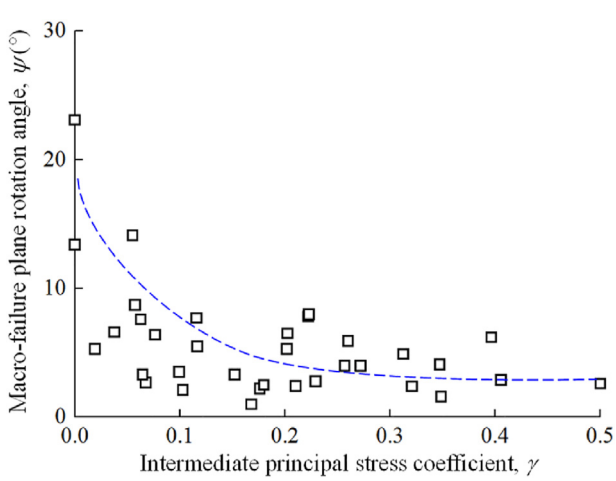

Fig. 6. Statistical relation between the macroscopic failure plane rotation angle ψ and intermediate principal stress coefficient γ. The blue dashed line is the trend line without fitting.

Table 1
Values of $(\mu/\beta)(\sigma_c/\sigma_t)$ and σ_c for different rock types.

Rock type	σ_c (MPa)	$(\mu/\beta)(\sigma_c/\sigma_t)$	R^2
Dunham dolomite (Mogi, 2006)	261.5	9.82	0.9954
Solnhofen limestone (Mogi, 2006)	310	4.69	0.9835
Yamaguchi marble (Mogi, 2006)	82	10.21	0.9976
Manazuru andesite (Mogi, 2006)	140	36.45	0.9932
Inada granite (Mogi, 2006)	229	30.15	0.9882
Orikabe monzonite (Mogi, 2006)	234	20.02	0.9794
Mizuho trachyte (Mogi, 2006)	100	11.23	0.9909
KTB amphibolite (Chang and Haimson, 2000)	164.7	30.11	0.9849
CJPL-II marble (Wang, 2020)	176	13.37	0.9851
Yunnan sandstone (Feng et al., 2019)	60	29.94	0.9994

Note: True triaxial compression tests of the CJPL-II marble were conducted in Wang (2020). More details about this rock type, the loading apparatus and the loading path can be found in previous studies (Zhao et al., 2018; Wang et al., 2020; Feng et al., 2021; Gao and Wang, 2021).

4. Relations between the most favorable direction and intermediate principal stress coefficient

In the previous section, Eq. (15) is derived for constant σ_2 and σ_3. Basically, φ_m is the most favorable direction angle between the wing crack opening direction and σ_3. In Eq. (15), when σ_3 keeps constant and σ_2 increases, as $(\mu/\beta)(\sigma_c/\sigma_t)$ is influenced by the constant material properties, σ_1 could increase. This contrasts with the test results where intermediate principal stress effects were observed in true triaxial compression test. It reveals that the strength increases at first and then decreases with the increase of σ_2 under constant σ_3. Therefore, φ_m should be related to the stress levels. As the stress level set $(\sigma_1, \sigma_2, \sigma_3)$ is in a vector space, which is hard to handle, a simple scalar named as the intermediate principal stress coefficient was proposed by Wang and Lade (2001). It is expressed as below:

$$\gamma = \frac{\sigma_2 - \sigma_3}{\sigma_1 - \sigma_3} \tag{16}$$

where γ is in the range of 0–1. When $\sigma_2 = \sigma_3$, we have $\gamma = 0$, which stands for the conventional triaxial compression. When $\sigma_1 = \sigma_2$, $\gamma = 1$, indicating the generalized conventional triaxial tension.

As Eq. (15) can stand for the strength of microcrack cluster, it can also reflect the characteristics of macro-failure. Hence, the macro-failure plane rotation angle ψ, which is the angle between the main failure plane and σ_2, is measured approximately, as shown in Fig. 5. Moreover, ψ is the angle between the opening direction of the main failure plane and σ_3, which is consistent with the definition of the rotation angle φ. It should be noted that ψ is calculated from a side view of the specimen and the spatial rotation is ignored.

The relation between ψ and the intermediate principal stress coefficient γ is shown in Fig. 6, in which the blue dashed line stands for the trend line. It can be observed from Fig. 6 that ψ seems to decrease with the increase of γ at a decreasing rate. ψ and γ have a negative exponential relationship, as reported in previous study (Chang and Haimson, 2005). It was pointed out that most of the microcrack orientations are random when $\sigma_2 = \sigma_3$, and they tend to be parallel to σ_2 direction as the differential stress $\sigma_2 - \sigma_3$ increases. Since φ_m is derivated from microcrack cluster, which reflects the feature of macro-failure to a certain extent, it can be assumed that φ_m follows the relation below:

$$\varphi_m = \varphi_0 e^{-D\gamma} \tag{17}$$

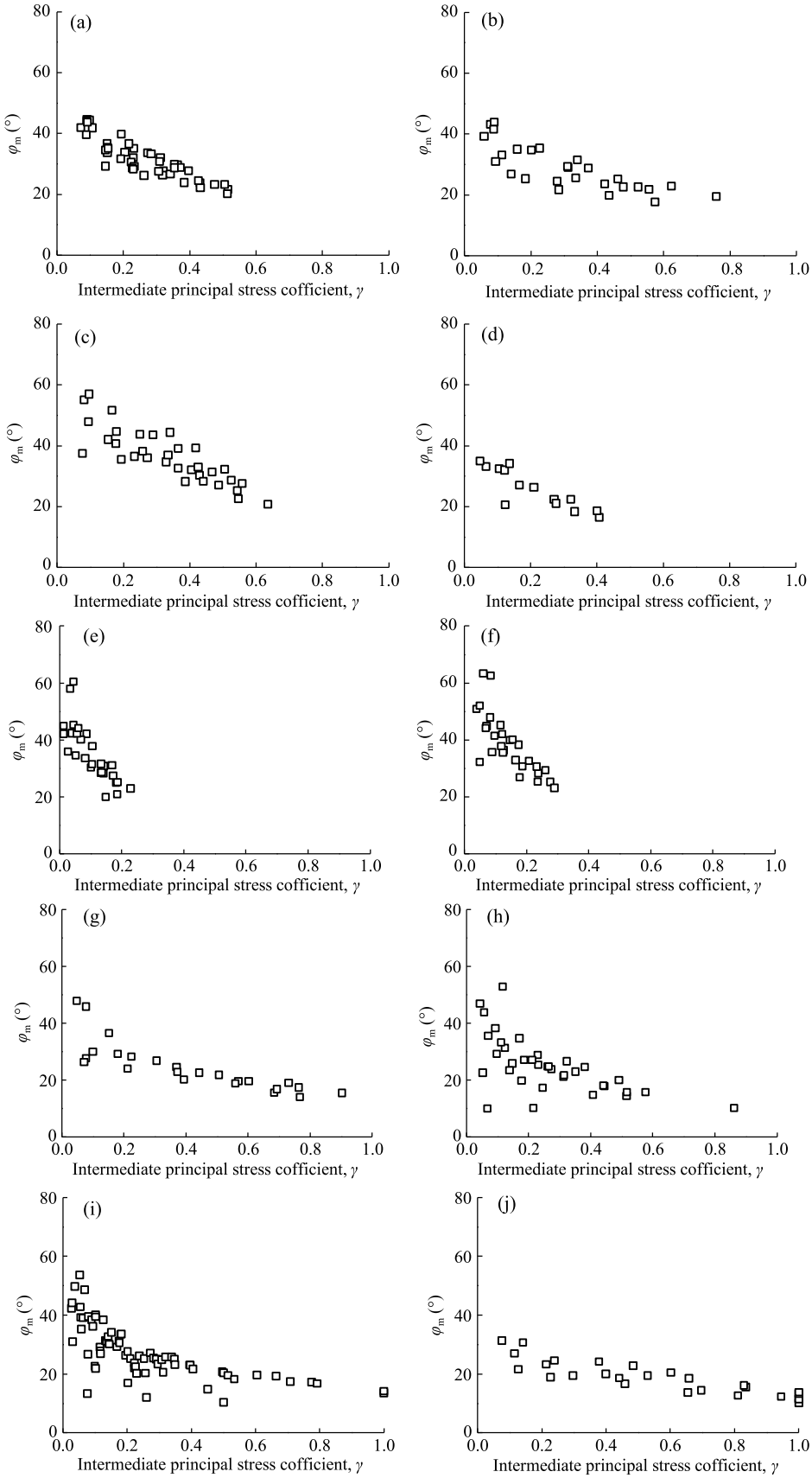

Fig. 7. Relations between the most advantageous direction angle φ_m and the intermediate principal stress coefficient γ for different rock types: (a) Dunham dolomite; (b) Solnhofen limestone; (c) Yamaguchi marble; (d) Manazuru andesite; (e) Inada granite; (f) Orikabe monzonite; (g) Mizuho trachyte; (h) KTB amphibolite; (i) CJPL-II marble; and (j) Yunnan sandstone.

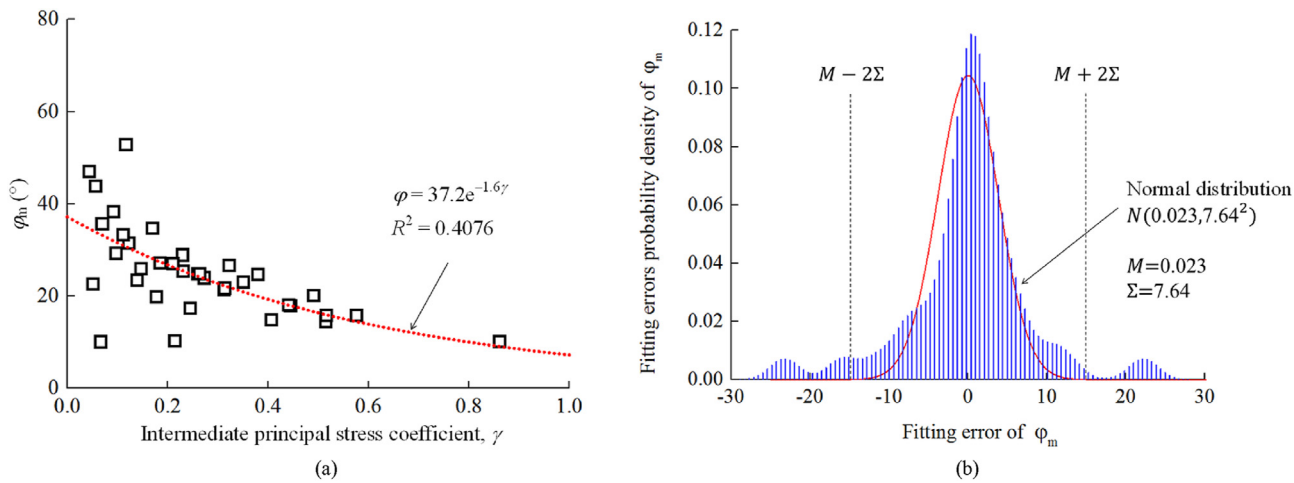

Fig. 8. Fitting result and errors of KTB amphibolite: (a) Fitting results of KTB amphibolite with an exponential function; and (b) Probability density histogram of the fitting error on the rotation angle φ_m. Besides, the best normal distribution is also illustrated.

where φ_0 is the initial favorable direction angle for $\gamma = 0$, and D is the attenuation rate.

The reasonability of Eq. (17) needs to be verified. Ten sets of published true triaxial tests on different types of intact rocks (Chang and Haimson, 2000; Mogi, 2006; Feng et al., 2019) have been taken for examining the accuracy of Eq. (17). Based on the uniaxial compression test results, the average σ_c is obtained. In addition, $(\mu/\beta)(\sigma_c/\sigma_t)$ is obtained from the best-fitting results according to the conventional compression data and Eq. (13), as shown in Table 1.

It can be seen that the results fit well in Table 1, indicating that Eq. (13) (derivative from Eq. (12)) can be applied for the uniaxial and conventional triaxial compression. With the reliability of σ_c and $(\mu/\beta)(\sigma_c/\sigma_t)$, φ_m can be calculated directly by Eq. (15). The relations between φ_m and the intermediate principal stress coefficient γ of different rocks are shown in Fig. 7.

It should be noted that φ_m was calculated directly from the experimental data and Eq. (15) without fitting. Eq. (17) was applied to fit the data, and the fitting results and errors of KTB amphibolite are shown in Fig. 8. The data are relatively discrete and the R^2 value is only 0.4076, as shown in Fig. 8a. It can be explained that the actual strength cannot be reached for a constant positive γ in real true triaxial compression tests, due to the variable experimental controlling conditions. Besides, there also exist errors during the experimental operation. In Fig. 8b, normal distribution is applied to fit the probability density histogram of the fitting errors, and Kolmogorov-Smirnov test condition is obtained. Hence, these experimental errors are random and accidental, which need to be abandoned for acquiring rational results. Thus, a computer program was written to abandon these random errors and determine the best-fitting solutions of the relation between φ_m and γ. Firstly, the data set was fitted roughly using the least square method and the misfit was calculated as well. The average value M and standard deviation Σ can be acquired. Afterward, the abnormal outlier data points (not in the range of $[M - 2\Sigma, M + 2\Sigma]$) were detected and eliminated based on the Pauta criterion. The remaining data were processed with the same method. It is worthy mentioning that iteration could be broken down when there were no outliers. The well fitted relation between φ_m and γ is shown in Fig. 9.

Fig. 9 indicates that Eq. (17) is suitable for different rocks after eliminating the accidental errors. The rock strength under any stress levels can be calculated by substituting Eq. (17) into Eq. (15):

$$\sigma_1 = \sigma_2 \sin^2\varphi_0 e^{-D\gamma} + \sigma_3 \cos^2\varphi_0 e^{-D\gamma} + \sqrt{\frac{\mu}{\beta}\frac{\sigma_c}{\sigma_t}\sigma_c\left(\sigma_2 \sin^2\varphi_0 e^{-D\gamma} + \sigma_3 \cos^2\varphi_0 e^{-D\gamma}\right) + \sigma_c^2} \quad (18)$$

When $\sigma_2 = \sigma_3$, Eq. (18) could be converted to Eq. (13), which is similar to the theoretical Hoek-Brown criterion (Zuo et al., 2008, 2015). Furthermore, Eq. (18) can be applied for true triaxial compression conditions.

5. Interpretation of the intermediate principal stress effect

The intermediate principal stress effect could be explained by Eq. (18), and its physical meaning is illustrated in this section.

Eq. (18) can be simplified as follows:

$$\sigma_1 = \sigma_* + \sqrt{\frac{\mu}{\beta}\frac{\sigma_c}{\sigma_t}\sigma_c\sigma_* + \sigma_c^2} \quad (19)$$

where σ_* is the equivalent stress, and $\sigma_* = \sigma_2 \sin^2\varphi_0 e^{-D\gamma} + \sigma_3 \cos^2\varphi_0 e^{-D\gamma}$. When $\sigma_2 = \sigma_3$, σ_* turns into σ_3, and Eq. (18) could be converted to Eq. (13).

In fact, the strength σ_1 increases monotonously with σ_*. The change of σ_* for a constant σ_3 is considered herein. Based on Eq. (17), φ_m decreases with the increase of γ, and the opening direction of microcrack cluster tends to be parallel to σ_1. Hence, the opening direction tendency of microcrack cluster is determined by the intermediate principal stress coefficient. For a constant σ_3, γ increases while φ_m decreases with the increase of σ_2, as shown in Fig. 10a. When σ_2 is larger than σ_3 and γ is larger than 0, φ_m and $\sin^2\varphi_m$ are large, causing that σ_* could increase with the increase of σ_2. When σ_2 is higher enough than σ_3 and γ is large, φ_m and $\sin^2\varphi_m$ could be relatively small. Hence, σ_* could decrease since the decrement of $\sin^2\varphi_m$ is much greater. Meanwhile, the strength will also start to decrease. However, when $\sigma_1 = \sigma_2$, the generalized conventional tensile strength is larger than the compressive strength in the condition that $\sigma_2 = \sigma_3$ as $\sigma_2 \sin^2\varphi_0 e^{-D} + \sigma_3 \cos^2\varphi_0 e^{-D}$ is larger than σ_3.

As shown in Fig. 10b, the calculated strength from Eq. (19) and the corresponding σ_* fit well with the experimental results. Hence, the intermediate principal stress effect can be revealed by Eq. (12)

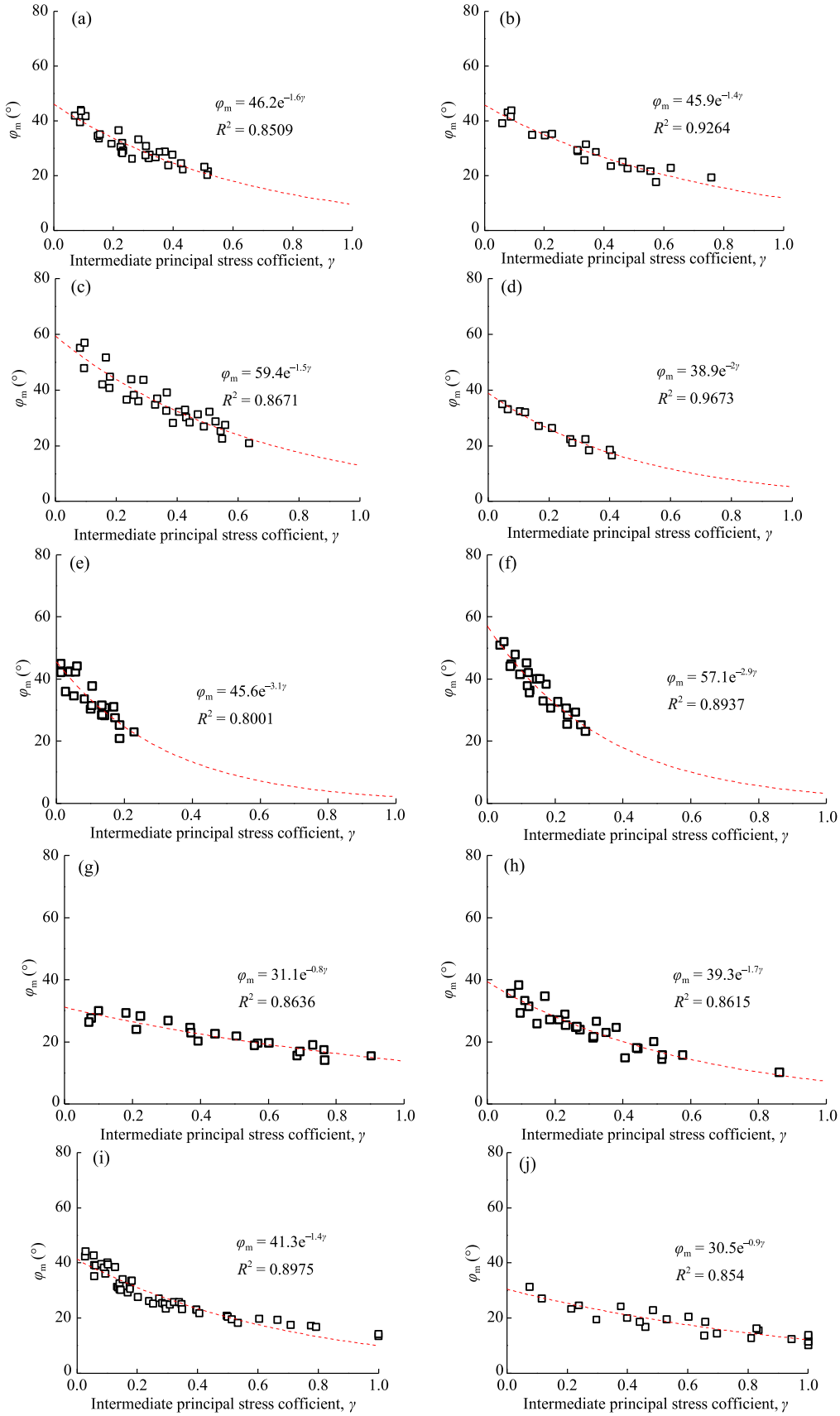

Fig. 9. Robust fitting relations between the most favorable direction angle φ_m and the intermediate principal stress coefficient γ for different rock types: (a) Dunham dolomite; (b) Solnhofen limestone; (c) Yamaguchi marble; (d) Manazuru andesite; (e) Inada granite; (f) Orikabe monzonite; (g) Mizuho trachyte; (h) KTB amphibolite,; (i) CJPL-II marble; and (j) Yunnan sandstone.

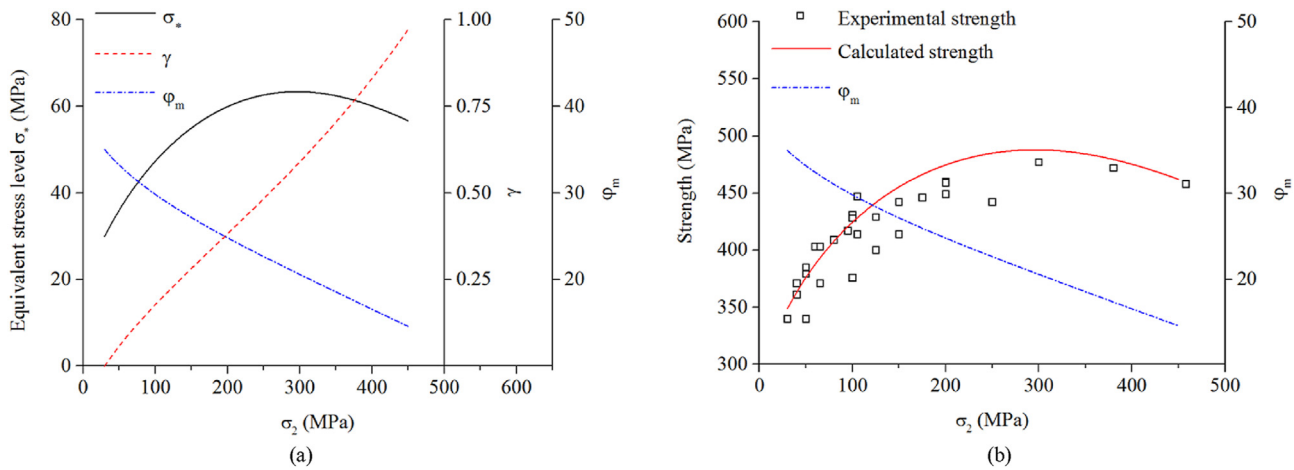

Fig. 10. (a) The equivalent stress σ_*, γ and φ_m against σ_2; and (b) Experimental and calculated strengths and φ_m against σ_2. The experimental results are acquired from the true triaxial compression tests of CJPL-II marbles for $\sigma_3 = 30$ MPa.

derived based on the fracture mechanics, Eq. (14) for strength measurement of microcrack cluster, and Eq. (17) for the stress level dependence of opening direction of microcrack cluster. Furthermore, it also indicates that the strength is influenced by the superposed effect of the stress levels and the stress level dependence of the opening direction φ_m of microcrack cluster in Eq. (17).

This interpretation can be linked to another distinct feature of true triaxial compression test results. Previous studies revealed that the final failure plane is approximately parallel to σ_2 direction (Mogi, 1981, 2006; Geng and Xu, 1985; Takahashi and Koide, 1989; Chang and Haimson, 2000; Chen and Feng, 2006; Feng et al., 2016) in true triaxial compression tests. As shown in Eq. (17), φ_m decreases and the opening direction of microcrack cluster tends to be parallel to σ_3 with the increase of γ. Accordingly, the marcocrack induced by the opening of the microcrack cluster tends to extend along σ_3 direction. In addition, the direction of final failure plane tends to be parallel to σ_2 with the increase of γ. The result

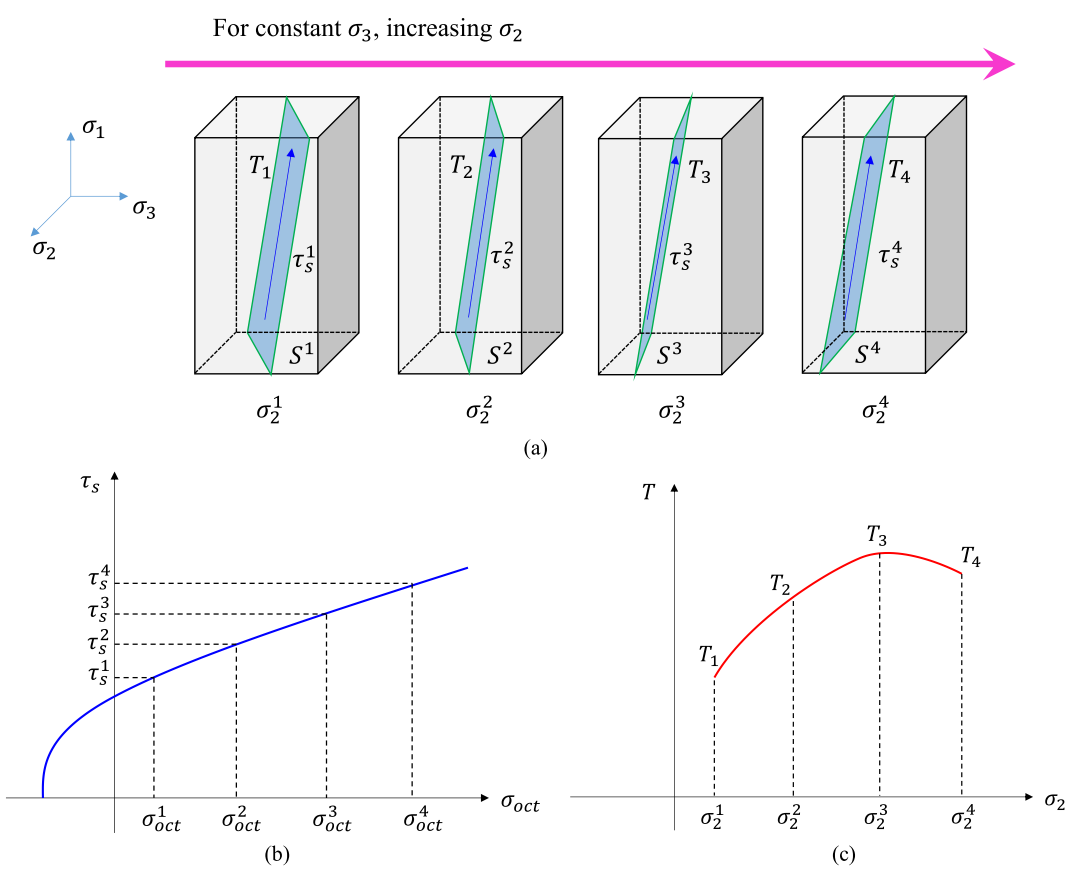

Fig. 11. Physical meaning of the strength and intermediate principal stress effect: (a) Different failure planes for different σ_2 levels (σ_2^1, σ_2^2, σ_2^3 and σ_2^4), where T_1, T_2, T_3 and T_4 are the tractions on the planes, S_1, S_2, S_3 and S_4 are the areas of the failure planes, and τ_s^1, τ_s^2, τ_s^3 and τ_s^4 are the shear strengths on the planes; (b) Shear strength τ_s plotted against the octahedral normal stress σ_{oct}; and (c) Traction T plotted against σ_2.

illustrated in Fig. 6 is consistent with the previous studies for a relatively high γ.

The physical meaning of the coupling effect is also clear to understand. As shown in Fig. 11a, T_1, T_2, T_3 and T_4 are the global traction forces on the final failure plane under different σ_2, S_1, S_2, S_3 and S_4 are the effective areas of the final failure plane, and τ_s^1, τ_s^2, τ_s^3 and τ_s^4 are the shear strengths of the failure plane. The failure condition of the failure plane can be calculated below:

$$\frac{T}{S} \geq \tau_s \tag{20}$$

In Fig. 11b, it can be seen that the shear stress τ_s always increases with the octahedral normal stress σ_{oct} ($\sigma_{oct} = (\sigma_1 + \sigma_2 + \sigma_3)/2$). For a constant σ_3, σ_{oct} increases with the increase of σ_2, resulting in $\tau_s^1 < \tau_s^2 < \tau_s^3 < \tau_s^4$, which indicates the influence of stress levels on the strength. When σ_3 is constant, the intermediate principal stress has little influence on the failure angle (the angle between σ_1 and the final failure plane) (Feng et al., 2019). Hence, the failure angle is set constant in Fig. 11a. Keeping σ_3 constant and increasing σ_2, the direction of final failure plane could tend to be parallel to σ_2 and then $S_1 > S_2 > S_3 > S_4$, which reveals the influence of the stress level dependence of the opening direction φ_m of microcrack cluster. Therefore, the coupling effect of stress level and the stress level dependence of the opening direction can be presented by Eq. (20), which is equivalent to Eq. (18). Moreover, Eq. (20) reveals the physical meaning of the coupling effect on the rock strength.

Based on Eq. (20), the real traction T required for failure can be calculated as $\tau_s S$. Due to $\tau_s^1 < \tau_s^2 < \tau_s^3 < \tau_s^4$ and $S_1 > S_2 > S_3 > S_4$, the maximum traction T may not be $\tau_s^4 S_4$ and could occur in a intermediate state. Fig. 11c shows a possible condition that T_3 is the maximum traction. The greater the real traction T required is, the larger the global strength there will be. Hence, the maximum strength could be reached with a mediate σ_2 and a constant σ_3. The physical meaning of this interpretation is illustrated as well.

Therefore, the rock strength is determined by the stress levels and the stress level dependence of the opening direction of microcrack cluster. The development of microcrack cluster is asymmetric, which could influence the strength. Besides, the development asymmetry is determined by the stress level. On one hand, the stress level can directly influence the strength; on the other hand, the intermediate principal stress can directly influence the asymmetric development of the microcrack cluster, leading to the variation of the strength.

6. Conclusions and discussion

In this paper, it is assumed that the failure of hard rocks is caused by the presence of penny-shaped microcracks. Based on the fracture mechanics and statistical analyses from existing true triaxial compression test results, a nonlinear 3D strength relation is proposed considering the effect of intermediate principal stress. Finally, the strength relation is applied to interpret the intermediate principal stress effect on the strength of hard rocks. The following conclusions are obtained:

(1) Based on the strength of microcrack cluster, a nonlinear 3D strength relation is proposed. Besides, the relation can be converted to the Hoek–Brown criterion when $\sigma_2 = \sigma_3$.
(2) The strength of hard rock is influenced by the coupled effect of stress level and the stress level dependence of the opening direction φ_m of microcrack cluster. With the increase of the intermediate principal coefficient γ, φ_m decreases in an empirical form, which can be verified by 10 kinds of hard rocks.
(3) The rock strength increases firstly and then decreases, which is induced by the direct effect of σ_2 strengthening coupled with the indirect effect of microcrack asymmetric development.

Furthermore, the physical meaning of the coupling effect can be explained by this nonlinear strength criterion and the interpretation of the intermediate principal stress effect. Actually, this strength relation can be considered as a 3D generalized Hoek–Brown criterion. However, it seems complex to be applied to the actual field conditions and should be simplified for convenience in the future. In addition, the physical meaning and determination method of the two added parameters need to be verified.

Declaration of competing interest

The authors declare that they have no known competing financial interests or personal relationships that could have appeared to influence the work reported in this paper.

Acknowledgments

The authors acknowledge the financial support the National Natural Science Foundation of China (Grant No. 52225404) and Beijing Outstanding Young Scientist Program (Grant No. BJJWZYJH01201911413037). We would also like to thank Key Laboratory of Ministry of Education on Safe Mining of Deep Metal Mines, Northeastern University, China for giving us the opportunities to conduct the experimental and simulating tests.

References

Aubertin, M., Simon, R., 1996. A multiaxial failure criterion that combines two quadric surfaces. In: The 2nd North American Rock Mechanics Symposium. American Rock Mechanics Association, Montreal, Canada.
Bobet, A., 2000. The initiation of secondary cracks in compression. Eng. Fract. Mech. 66 (2), 187–219.
Böker, R., 1915. Die Mechanik der bleibenden Formänderung in kristallinisch aufgebauten Körpern Verhandel. Selbstverl. d. Vereines Dt. Ingenieure, Berlin, Germay (in German).
Brown, E.T., 2015. Editorial. J. Rock Mech. Geotech. Eng. 7 (4), 359–360.
Cai, M., Hou, P.Y., Zhang, X.W., Feng, X.T., 2021. Post-peak stress–strain curves of brittle hard rocks under axial-strain-controlled loading. Int. J. Rock Mech. Min. Sci. 147, 104921.
Chang, C., Haimson, B., 2000. True triaxial strength and deformability of the German Continental Deep Drilling Program (KTB) deep hole amphibolite. J. Geophys. Res. Solid Earth 105 (B8), 18999–19013.
Chang, C., Haimson, B., 2012. A failure criterion for rocks based on true triaxial testing. Rock Mech. Rock Eng. 45, 1007–1010.
Chang, C., Haimson, B., 2005. Non-dilatant deformation and failure mechanism in two Long Valley Caldera rocks under true triaxial compression. Int. J. Rock Mech. Min. Sci. 42 (3), 402–414.
Chen, J., Feng, X.T., 2006. True triaxial experimental study on rock with high geostress. Chin. J. Rock Mech. Eng. 25 (8), 1537–1543 (in Chinese).
Ewy, R.T., 1999. Wellbore-stability predictions by use of a modified Lade criterion. SPE Drill. Complet. 14 (2), 85–91.
Feng, X.T., Zhang, X., Kong, R., Wang, G., 2016. A novel Mogi type true triaxial testing apparatus and its use to obtain complete stress–strain curves of hard rocks. Rock Mech. Rock Eng. 49, 1649–1662.
Feng, X.T., Kong, R., Zhang, X., Yang, C., 2019. Experimental study of failure differences in hard rock under true triaxial compression. Rock Mech. Rock Eng. 52, 2109–2122.
Feng, X.T., Wang, Z., Zhou, Y., Yang, C., Pan, P.Z., Kong, R., 2021. Modelling three-dimensional stress-dependent failure of hard rocks. Acta Geotech 16, 1647–1677.
Gao, Y., Wang, Z., 2021. Experimental study on the damage process of marble under true triaxial pre-peak unloading conditions. Int. J. Damage Mech. 30 (10), 1542–1557.
Geng, N., Xu, D., 1985. Rock rapture caused by decreasing the minimum principal stress. Acta Geophys. Sin. 28 (2), 191–197.
Griffith, A.A., 1921. The phenomena of rupture and flow in solids. Philos. Trans. R. Soc. Lond. Ser. A – Math. Phys. Eng. Sci. 221 (582–593), 163–198.
Hoek, E., Brown, E.T., 1980. Underground Excavations in Rock. Institute of Mining and Metallurgy, London, UK.

Hoek, E., Brown, E.T., 2019. The Hoek–Brown failure criterion and GSI – 2018 edition. J. Rock Mech. Geotech. Eng. 11 (3), 445–463.
Horii, H., Nemat-Nasser, S., 1986. Brittle failure in compression: splitting faulting and brittle-ductile transition. Philos. Trans. R. Soc. Lond. Ser. A – Math. Phys. Eng. Sci. 319 (1549), 337–374.
Jaeger, J.C., Hoskins, E.R., 1966. Rock failure under the confined Brazilian test. J. Geophys. Res. 71 (10), 2651–2659.
Jaeger, J.C., Cook, N.G.W., Zimmerman, R., 2007. Fundamentals of Rock Mechanics, fourth ed. Wiley-Blackwell, London, UK.
Kachanov, M.L., 1982. A microcrack model of rock inelasticity part II: propagation of microcracks. Mech. Mater. 1 (1), 29–41.
Ma, X., Rudnicki, J.W., Haimson, B.C., 2017. The application of a Matsuoka-Nakai-Lade-Duncan failure criterion to two porous sandstones. Int. J. Rock Mech. Min. Sci. 92, 9–18.
McClintock, F.A., Walsh, J.B., 1962. Friction on Griffith cracks in rocks under pressure. In: Proceedings of the 4th U.S. National Congress of Applied Mechanics. American Society of Mechanical Engineers (ASME), New York, USA, pp. 1015–1021.
Mogi, K., 1967. Effect of the intermediate principal stress on rock failure. J. Geophys. Res. 72 (20), 5117–5131.
Mogi, K., 2006. Experimental Rock Mechanics. CRC Press, London, UK.
Mogi, K., 1971. Fracture and flow of rocks under high triaxial compression. J. Geophys. Res. 76 (5), 1255–1269.
Mogi, K., 1981. Flow and fracture of rocks under general triaxial compression. Appl. Math. Mech. – Engl. Ed. 2 (6), 635–651.
Murrell, S.A.F., 1965. The effect of triaxial stress systems on the strength of rocks at atmospheric temperatures. Geophys. J. Int. 10 (3), 231–281.
Nuismer, R.J., 1975. An energy release rate criterion for mixed mode fracture. Int. J. Fract. 11 (2), 245–250.
Pan, P.Z., Feng, X.T., Hudson, J.A., 2012. The influence of the intermediate principal stress on rock failure behaviour: a numerical study. Eng. Geol. 124, 109–118.
Paterson, M.S., Wong, T., 2005. Experimental Rock Deformation – the Brittle Field, second ed. Springer-Verlag, Berlin, Heidelberg, New York.
Rafiei Renani, H., Cai, M., 2022. Forty-year review of the Hoek–Brown failure criterion for jointed rock masses. Rock Mech. Rock Eng. 55, 439–461.
Sih, G.C., Macdonald, B., 1974. Fracture mechanics applied to engineering problems-strain energy density fracture criterion. Eng. Fract. Mech. 6 (2), 361–386.
Tada, H., Paris, P.C., Irwin, G.R., 1973. The Stress Analysis of Cracks. Del Research Corporation, Hellertown, USA.
Takahashi, M., Koide, H., 1989. Effect of the intermediate principal stress on strength and deformation behavior of sedimentary rocks at the depth shallower than 2000 m. In: Maury, V., Fourmaintraux, D. (Eds.), Rock at Great Depth: Proceedings of International Symposium on Rock at Great Depth. A.A. Balkema, Rotterdam, Netherlands.
Tapponnier, P., Brace, W.F., 1976. Development of stress-induced microcracks in Westerly granite. Int. J. Rock Mech. Min. Sci. Geomech. Abstr. 13 (4), 103–112.
Wang, E.Z., Shrive, N.G., 1993. Brittle fracture in compression: mechanisms, models and criteria. Eng. Fract. Mech. 46 (1), 15–26.
Wang, H., Dyskin, A., Pasternak, E., Dight, P., Sarmadivaleh, M., 2018. Effect of the intermediate principal stress on 3D crack growth. Eng. Fract. Mech. 204, 404–420.
Wang, H., Dyskin, A., Pasternak, E., 2019. Comparative analysis of mechanisms of 3D brittle crack growth in compression. Eng. Fract. Mech. 220, 106656.
Wang, Q., Lade, P.V., 2001. Shear banding in true triaxial tests and its effect on failure in sand. J. Eng. Mech. 127 (8), 754–761.
Wang, Z., Feng, X.T., Yang, C., Zhou, Y., Han, Q., Gao, Y., 2020. Experimental investigation on fracturing process of marble under biaxial compression. J. Rock Mech. Geotech. Eng. 12 (5), 943–959.
Wang, Z., 2020. Modelling Elastic-Plastic-Ductile-Brittle Behaviours of Hard Rocks under Three-Dimensional Stress. University of Chinese Academy of Sciences.
Wiebols, G.A., Cook, N.G.W., 1968. An energy criterion for the strength of rock in polyaxial compression. Int. J. Rock Mech. Min. Sci. Geomech. Abstr. 5 (6), 529–549.
Zhang, L., Zhu, H., 2007. Three-dimensional Hoek–Brown strength criterion for rocks. J. Geotech. Geoenviron. Eng. 133 (9), 1128–1135.
Zhao, J., Feng, X.T., Zhang, X.W., Zhang, Y., Zhou, Y.Y., Yang, C.X., 2018. Brittle- ductile transition and failure mechanism of Jinping marble under true triaxial compression. Eng. Geol. 232, 160–170.
Zhou, X.P., Shou, Y.D., Qian, Q.H., Yu, M.H., 2014. Three-dimensional nonlinear strength criterion for rock-like materials based on the micromechanical method. Int. J. Rock Mech. Min. Sci. 72, 54–60.
Zuo, J.P., Li, H.T., Xie, H.P., Ju, Y., Peng, S.P., 2008. A nonlinear strength criterion for rock-like materials based on fracture mechanics. Int. J. Rock Mech. Min. Sci. 45 (4), 594–599.
Zuo, J.P., Liu, H., Li, H.T., 2015. A theoretical derivation of the Hoek–Brown failure criterion for rock materials. J. Rock Mech. Geotech. Eng. 7 (4), 361–366.
Zuo, J.P., Shen, J.Y., 2020. The Hoek–Brown Failure Criterion – from Theory to Application. Springer, Singapore.

Jianping Zuo obtained his MSc and PhD degrees from China University of Mining and Technology (Beijing), China. He is Professor and Dean of the School of Mechanics and Civil Engineering, China University of Mining and Technology (Beijing). He has been involved in the research on mining rock mechanics and rock strata control engineering, consulting and teaching for more than 20 years. He has been in charge of and/or participated in more than 40 scientific research projects, which were funded by the National Natural Science Foundation of China (NSFC), National Basic Research Program of China (973 Program), Beijing Major Scientific and Technological Achievements into Ground Cultivation Project, the 111 Project and Coal Mines Corporations. He is the author or co-author of more than 200 scientific papers. He received 31 national patents, and 12 Natural Science and Technology Progress Awards. In recent years, he has been awarded National Excellent Doctoral Dissertation Award (2009), New Century Excellent Talents of the Ministry of Education (2009), Fok Excellent Young Teachers Award (2014), Outstanding Young Talents of "Ten Thousand People Plan" (2015), Outstanding Young Science Foundation by NSFC (2016), Young Changjiang Scholar of Ministry of Education (2017), the first Young Outstanding Teacher in Beijing (2017), the Beijing Excellent Young Scientists (2019) and Science Achievement Award of International Society for Rock Mechanics and Rock Engineering (ISRM) (2020), and the National Science Fund for Distinguished Young Scholars (2022).